ELSEVIER

Thermochimica Acta 284 (1996) 1–19

thermochimica acta

# Modulated differential scanning calorimetry in the glass transition region. Part III. Evaluation of polystyrene and poly(ethylene tetrephthalate)[1]

Andreas Boller[a,b], Iwao Okazaki[a,b,2], Bernhard Wunderlich[a,b],

[a] *Department of Chemistry, The University of Tennessee, Knoxville, TN 37996-1600, USA*
[b] *Chemistry and Analytical Sciences Division, Oak Ridge National Laboratory, Oak Ridge, TN 37831-6197, USA*

**Abstract**

Modulated differential scanning calorimetry (MDSC)) presents a new method to evaluate the kinetics underlying the glass transition. Equations that were derived earlier to describe the various time effects in the glass transition, based on irreversible thermodynamics and the theory of liquids, are applied to quasi-isothermal MDSC experiments on amorphous polystyrene and poly(ethylene terephthalate). The analysis involves the computation of a phase angle for the change in the apparent heat capacity at the glass transition that becomes 60° at the point of half-vitrification, followed by a determination of the activation energy as a function of modulation amplitude. Activation energies of 346 and 328 kJ $mol^{-1}$ were found for the respective polymers.

*Keywords:* Activation energy; Glass transition; Heat capacity; Heat flow calorimeter; MDSC; Modulated calorimetry; Poly(ethylene terephthalate); Polystyrene; Thermodynamics

## 1. Introduction

This series of publications was begun with a qualitative analysis of the glass transition of polystyrene by modulated differential scanning calorimetry (MDSC) [1].

* Corresponding author.

[1] Presented at the 24th North American Thermal Analysis Society Conference, San Francisco, CA, U.S.A., 10–13 September 1995

[2] On leave from Toray Industries, Inc, Otsu, Shiga 520, Japan.


*PII* S0040-6031(96)02865-1

As pointed out already in the first papers on MDSC [2], the glass transition and the enthalpy relaxation could be separated by recording the reversing and total heat flows of a measurement at a fixed, underlying heating rate $< q >$. The MDSC is used in such measurements with two time scales, a fast one, fixed by the modulation time period, and a slow one, fixed by $< q >$. It could be documented that MDSC can in these cases determine the glass transition temperature as largely independent of the thermal history and the (slow) heating or cooling rates, but that the measurement is dependent on the (fast) modulation frequency [1]. It could, further, be shown that the frequency dependence seems similar to the effect measured by dynamic mechanical analysis (DMA), but that the loss peak in DMA occurs at a higher temperature than the glass transition temperature, $T_g$, as measured by MDSC at the same frequency [1]. Small differences in the appearance of the glass transitions exist between samples of different thermal history and measurements performed on heating or cooling. Both these secondary effects will be addressed in part IV of this series of paper [3]. They are caused by differences in the glassy structure with thermal history and the interaction between the different time scales of modulation and underlying heating rate. In the second part of this series of papers on the MDSC of the glass transition, the mathematical basis for the description of the kinetics was given [4]. The results of paper II will be used for the analysis of the quasi-isothermal analysis presented in this paper.

The MDSC used in this research is modulated at the block temperature $T_b(t)$ with a sinusoidally changing amplitude that is governed, as in standard DSC, by the temperature measured at the sample position. The measurements are carried out in a quasi-isothermal mode, *i.e.* without an underlying heating rate, so that the data are free of interference from an underlying heating rate $< q >$. The block or furnace temperature is given by

$$T_b(t) = T_0 + A_{T_b} \sin \omega t \tag{1}$$

where $T_0$ is the isotherm at the beginning of the experiment, which is changed for each measured point (quasi-isothermal experiments [5]). The modulation frequency $\omega$ is equal to $2\pi/p$ in units of rad $s^{-1}$, with $p$ representing the duration of one cycle. Measurements can then be made as soon as steady state is reached. The sample and reference temperatures, $T_s$ and $T_r$, respectively, are given at steady state by

$$T_s = T_0 + A_{T_s} \sin(\omega t - \varepsilon) \tag{2}$$

$$T_r = T_0 + A_{T_r} \sin(\omega t - \phi) \tag{3}$$

where $A_{T_s}$ and $A_{T_r}$ are the modulation amplitudes, and $\varepsilon$ and $\phi$ are the phase lags at the sample and reference positions ($A_{T_s} = A = A_{T_b} \cos \varepsilon$, set at the chosen modulation amplitude; and $A_{T_r} = A_{T_b} \cos \phi$). The heat capacity is next computed from Eqs. (2) and (3) to be [6]

$$mc_p = \frac{A_\Delta}{A_{T_s}} \sqrt{\left(\frac{K}{\omega}\right)^2 + C'^2} = \frac{A_\Delta}{A_{T_s}} K' \tag{4}$$

where $m$ is the sample mass, $c_p$ the specific heat capacity of the sample, $A_\Delta$ the amplitude of the temperature difference, proportional to the heat flow, $K$ the frequency-indepen-

dent Newton's Law Constant, $C'$ the heat capacities of the empty samples and reference calorimeters of identical weights. The constant $K'$ is the frequency-dependent calibration constant, to be evaluated for the given measuring frequency and empty pan with heat capacity $C'$.

Before the resulting data can be analyzed, it must be ascertained that the initial instrument lag has decayed and the instrument remains in steady state during the time interval of measurement, *i.e.* any measured time effect is due to the sample and not due to the thermal conductivity that causes the lags $\varepsilon$ and $\phi$ of Eqs. (2) and (3). Detailed discussions of the lags were given in Ref. [7] and the estimated limits will be applied to the experimental data.

## 2. Experimental details

### 2.1. Instrumentation, calibration, and measurements

A commerical Thermal Analyst 2910 system from TA Instruments Inc. with modulated DSC (MDSC) was used for the measurements on polystyrene. Dry $N_2$ gas with a flow rate of 10 ml $min^{-1}$ was purged through the sample. Cold nitrogen, generated from liquid nitrogen was used for cooling. The sample mass was about 5.9 mg. For poly(ethylene terephthalate), a Thermal Analyst 2920 MDSC was employed with dry $N_2$ gas with a flow rate of 30 ml $min^{-1}$. Cooling was accomplished with the refrigerated cooling system (RCS) to $-80$°C. The sample mass was about 5.0 mg. For calibration of both sample runs, 24.9 mg of sapphire were used [8]. The pan weights were always about 23 mg and matched on sample and reference sides. It was made sure that the modulation amplitude of the sample temperature $A$ was chosen so that steady state could be maintained within the changes in heating rates produced during the modulation. For detailed graphs of the limits of modulation as a function of temperature and cooling capacity, see Ref. [5]. Temperature calibration was carried at the onsets of the transition peaks for cyclohexane (186.1 and 279.7K), napthalene (353.42 K), indium (429.75 K) and tin (505.05 K).

The experiments were carried out quasi-isothermally. For polystyrene, measurements were made at 24 temperatures covering the glass region starting at about 400 K and finishing at about 340 K. The same maximum heating and cooling rates of 3.8 K $min^{-1}$ were set in the modulation by using the amplitudes $A = 0.3$, 0.6, and 1.0 K, coupled with periods $p$ of 30, 60, and 99 s, respectively (frequencies $\omega = 0.121$–$0.06$ rad $s^{-1}$). For poly(ethylene terephthalate), the temperature range was 320–390 K in steps of 2 K, $A$ was set to 0.5, 1, 0 and 1.5 K, coupled to periods of 30, 60, and 90 s, giving a maximum heating rate of 6.3 K $min^{-1}$.

### 2.2. Sample description

The atactic PS was a standard sample of MW = 100,000 Da, $M_w/M_n < 1.06$. It was bought from Polyscience. Inc., Warrington, PA. The heat capacity of such standard polystyrene is available in the ATHAS data bank [9] and the kinetics of the glass

transition temperature $T_g$ is 373 K for the typical cooling rates of 1–10 K $min^{-1}$. The increase in heat capacity at $T_g$ is 30.8 J $K^{-1}$ $mol^{-1}$ for the repeating unit of 104.2 Da. The change in $T_g$ with cooling rate found to be 4.03 $\log q$ ($q$ in K $min^{-1}$) [10].

The PET was a typical industrial sample (Toray Ind.) of viscosity average molar mass of 18,000 Da (intrinsic viscosity of 0.615 dl $g^{-1}$ in ortho-chlorophenol). The PET was quenched in liquid nitrogen to be fully amorphous for the analyses. The data bank values for $T_g$ and the increase in heat capacity at $T_g$, $\Delta C_p$, are 342 K and 77.8 J $K^{-1}$ $mol^{-1}$, respectively, for the repeating unit of 192.2 Da [9].

### 2.3. Data treatment and lag estimate

The recording and deconvolution of the signals described by Eqs. (2) and (3) is done by the software of the chosen MDSC. Details are given, for example, in Refs. [5] and [6]. For both samples, each quasi-isothermal run took about 20 min of which the last 10 min were used for data collection. A typical recording of the sample temperature and heat flow as a function of time is given in Fig. 1. The Lissajous figures indicate an attainment of steady state within two to four modulation periods. An estimation of the heat capacity of the sample $C_s (= mc_p + C')$ divided by the Newton's Law constant $K$ is less than 1.0 s. (see Eq. (4)). The maximum lag $\Lambda$ due to the instrument operating at a heating rate $q$ with a continuous change in $C_s$ is given in Ref. [7] and can be written as

$$\Lambda = < q > \left(\frac{dC_p}{dT}\right) C_s/K \tag{5}$$

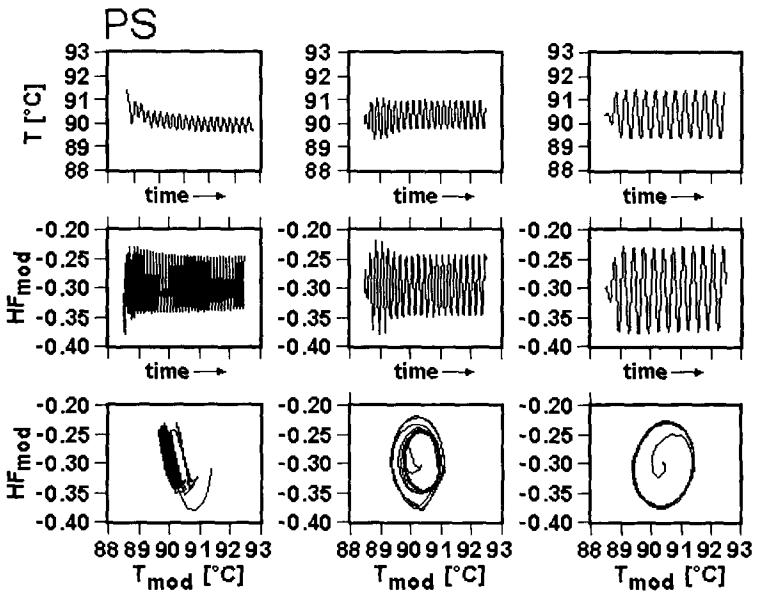


Fig. 1. Recording of the measured values of $T_s$ and $HF$ (proportional to $\Delta T$) for polystyrene in the glass transition region at different frequencies. The bottom curves are the corresponding Lissajous figures.

Assuming $dC_p/dT$ is 5%/K in the glass transition region and the modulation stays at a heating rate of 6 K $min^{-1}$, the instrumental lag is less than 0.5%, well within the error limit.

## 3. Theory of the kinetics of the glass transition

Below the glass transition temperature $T_g$, the heat capacity $C_p$ consists practically only of vibrational contributions. From molecular dynamics simulations, one can show that steady state for the vibrations in solids is reached in picoseconds ($10^{-12}$ s) [11] and one can, thus, represent the solid heat capacity by its vibrational, time-independent contribution $C_{p_0}$

$$C_p(\text{solid}) = C_{p_0} \tag{6}$$

This vibrational heat capacity is available through the Advanced Thermal Analysis System, ATHAS [9]. In the liquid state, longer times are necessary to reach thermal equilibrium beacuse of the need of the molecules to undergo additional, cooperative, structure changes. Again, values are available through ATHAS. In the glass transition region, both liquid and solid heat capacities are available by extrapolation. A simple model for the representation of the liquid heat capacity has been given by Eyring and Frenkel [12] in terms of a hole theory, *i.e.* the larger expansivity of liquids and the slower response to external forces is taken to be due to a temperature-dependent change in an equilibrium of holes of equal sizes. The equilibrium number of holes is $N^*$, and each mole of holes contributes an energy $\varepsilon_h$ to the enthalpy. The hole contribution of the heat capacity is then given by the change in the number of holes with temperature under equilibrium conditions [10]. The total heat capacity is then

$$C_p(\text{liquid}) = C_{p_0} + \varepsilon_h\left(\frac{dN^*}{dT}\right) \tag{7}$$

The creation, motion, and destruction of holes are the slow, cooperative, processes. Deviations from Eq. (7) occur if the measurement is carried out faster than the kinetics of the changes in the number of holes.

The hole theory can be applied to the glass transition by considering the kinetics of hole formation [13]. One can write a simple, first-order kinetics expression [10]

$$\left(\frac{dN}{dt}\right) = \frac{1}{\tau}(N^* - N) \tag{8}$$

with $N$ representing the instantaneous number of holes, $N^*$ the equilibrium number of holes, and $\tau$ the relaxation time for the formation of holes. For both $N^*$ and $\tau$, more detailed expressions are available through the hole theory [10]. Eq. (7) can be used to describe the apparent, time-dependent heat capacity, $C_p^{\#}$, by replacing $dN^*/dT$ with $(dN/dt) \times (dt/dT)$. Eq. (8) can also be derived from other represention of the time dependence of the glass transition. Most general would be the use of irreversible thermodynamics. In this case, $1/\tau$ is proportional to the curvature of the free energy relative to the relaxing internal variable at equilibrium [14].

The solution of Eq. (8) was given earlier [10] as

$$N(t) = N(t_0)e^{-\Phi(t)} + e^{-\Phi(t)} \int_{t_0}^{t} \frac{N^*(t')}{\tau(t')} e^{\Phi(t)} dt'$$

$$\Phi(t) = \int_{t_0}^{t} \frac{1}{\tau(t')} dt' \tag{9}$$

where $t_0$ is the beginning of the experiment, and $\Phi(t)$ is the time-integrated relaxation time. Both $\tau$ and $N^*$ are to be inserted into Eq. (9) with their proper temperature and (through the modulation) time dependence.

For the temperature dependence over the small modulation amplitude, one can assume that $\tau$ has an Arrhenius-type temperature dependence, $\tau = B\exp \varepsilon_j/(RT)$. From the hole theory, a detailed expression is available for $B$ in terms of the partition functions of the hole configuration [10]. With the modulation $T = T_0 + A\sin \omega t$, the time dependence of $\tau$ can be written as

$$\tau(t') = Be^{\varepsilon_j/RT_0(1 + A/T_0 \sin \omega t')^{-1}} \tag{10}$$

with $T_0$ representing the quasi-isothermal base temperature. This expression needs to be inserted into the expression for $\Phi(t)$. For small modulation amplitudes, it could be shown that Eq. (10) yields at long times, such as the 10 min chosen in the present experiments, $\Phi(t) \approx (t - t_0)/\tau$.

For the derivation of the expression with modulation affecting the number of holes $N^*$ and also the relaxation time $\tau$, two normalized, dimensionless modulation amplitudes are introduced to describe the changes in $N$ and $\tau$ respectively

$$A_N = \frac{A\alpha}{N_0^*} \quad \text{and} \quad A_\tau = \frac{A\varepsilon_j}{RT_0^2} \tag{11}$$

where $A$ is the amplitude, set for the temperature modulation, and $\alpha$ the change of $N^*$ with temperature ($= dN^*/dT$). *With* $t_0 = 0$, Eq. (9) becomes [7]

$$N(t) = N_0 e^{-t/\tau_0} + e^{-t/\tau_0} \int_0^t \frac{N_0^*(1 + A_N \sin \omega t')}{\tau_0(1 - A_\tau \sin \omega t')} e^{-t/\tau_0} dt' \tag{12}$$

The solution of Eq. (12) is rather involved in this form [7], but it is possible to solve it for $A_\tau$ approaching zero. The solution includes two components, one with the phase angle $\gamma$, given by

$$\cos \gamma = \frac{\dfrac{1}{\tau_0}}{\sqrt{\left(\dfrac{1}{\tau_0}\right)^2 + \omega^2}} \tag{13}$$

and the other with a phase angle of $2\beta$, related to $\gamma$, and given by

$$\cos 2\beta = \frac{\dfrac{1}{\tau_0}}{\sqrt{\left(\dfrac{1}{\tau_0}\right)^2 + 4\omega^2}} = \frac{\cos \gamma}{\sqrt{4 - 3\cos^2 \gamma}} \tag{14}$$

The steady state solution is given by [7].

$$N - N_0^* = N_0^* \left[ \frac{A_N A_\tau}{2} + (A_N + A_\tau)\cos\gamma \sin(\omega t - \gamma) - \frac{A_N A_\tau}{2}\cos 2\beta \cos 2(\omega t - \beta) \right] \quad (15)$$

With Eq (15) the apparent increase in heat capacity at the glass transition $\Delta C_p^\#$ can be computed. The differential $d(N_0^* - N)/dt$ multiplied by $\varepsilon_h$ is equal to the heat flow caused by the change in the number of holes. The differential $dt/dT$ is $(1/A\omega)[1/\cos(\omega t - \varepsilon)]$ as can be seen from Eq. (2). At steady state, the ratio of the two amplitudes is the reversing heat capacity signal recorded by the MDSC

$$\Delta C_p^\# = \frac{N_0^* \varepsilon_h}{A}[(A_N + A_\tau)\cos\gamma + A_N A_\tau \cos 2\beta)] \quad (16)$$

Note that the first term of Eq. (15) is not modulated and thus, does not contribute to the reversing $\Delta C_p^\#$, and that, because of the overall linearity of the system, the various contributions to the heat capacity are additive. The total, apparent heat capacity is, finally, $C_p^\# = C_{p_o} + \Delta C_p^\#$.

The measurements on PS and PET revealed that in this glass transition region $A_\tau$ is about 100 times larger than $A_N$, violating the condition for the solution of Eq. (12). In this case, Eq. (8) can be solved conveniently as a sufficiently finely spaced difference equation, evaluating $N$ by continuous summation from $N_0$ set at the starting time [10]. This $N_0$ is the parameter determining the thermal history for the sample. Its change towards equilibrium is only recognized as a reversing contribution as far as it can be modulated by the change in the equilibrium number of holes. Its average change during the modulation cycle causes a nonreversing contribution [4, 7].

The activation energy $\varepsilon_j$ is found from the experimental data by evaluation of Eq. (12) for a constant, average relaxation time $\tau_0$. Inserting $A_\tau = 0$ into Eq. (16) leads to the equation

$$\Delta C_p^\# = \Delta C_{p_o} \cos\gamma' \quad (17)$$

The glass transition defined as the point of half-vitrification [15], occurs at $\gamma' = 60°$. From Eq. (13) an approximate relaxation time $\tau_0'$ can be obtained, and from a plot of $\log\tau_0'$ vs. $1/T_0$, the activation energy $\varepsilon_j'$ determined. Extrapolation of $\tau_0'$ to zero amplitude $A$ yields the activation energy $\varepsilon_j$ and permits the calculation of $A_\tau$. Finally, $A_N$ can be computed from Eqs. (11) and (16) for $\gamma = 0$.

## 4. Results

### 4.1. Measured data

The raw data of the heat capacities were corrected to the calibrated temperature and the increase in heat capacity was normalized to 100% ( $= \Delta C_{p_o}$ ) as shown in Figs. 2 and 3. The numerical values are listed in Tables 1 and 2. The heat capacity was evaluated

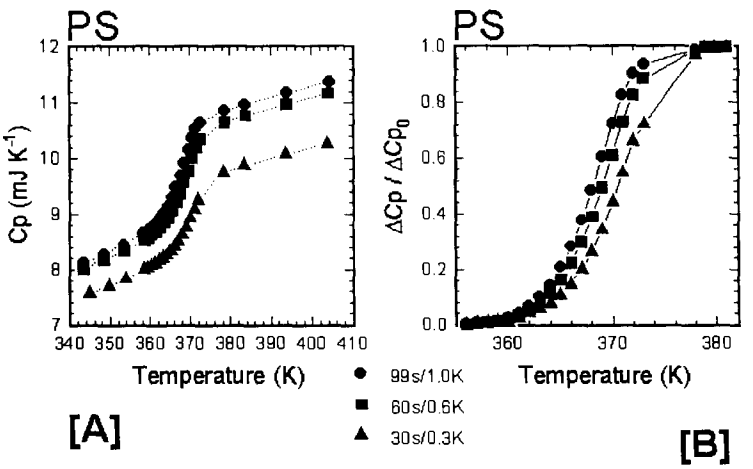


Fig. 2. [A] Uncalibrated, steady state, reversing, apparent heat capacities of polystyrene at different frequencies. [B] Data recalculated as fraction of the change of heat capacity at the glass transition.

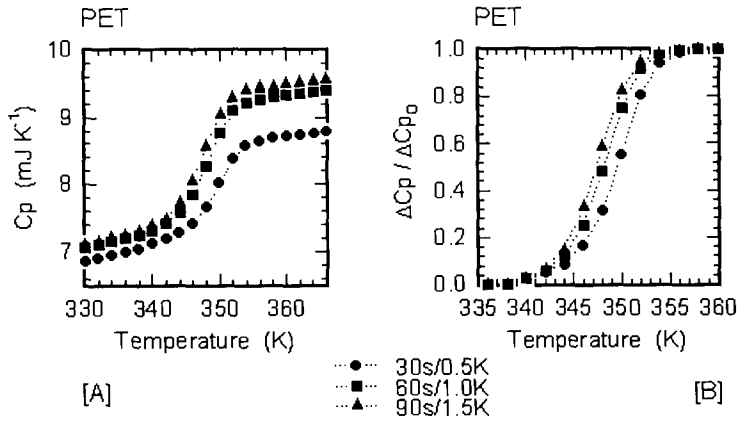


Fig. 3. [A] Uncalibrated, steady state, reversing, apparent heat capacities of poly(ethylene terephthalate) at different frequencies. [B] Data recalculated as fraction of the change of heat capacity at the glass transition.

every 0.2 s and accumulated for 3 s, to give for each recorded point an average of 15 measurements. Over the 10 min data collection 200 such points were recorded and averaged, removing any statistical error. An example of the quality of the PET data can be gained from the Lissajous figures in Fig. 4 which represent the runs at a period of 60 s and amplitude of 1 K at four selected temperatures within the glass transition region. Each figure represents a superposition of 10 modulation cycles and is, thus, based on the 3,000 heat-flow evaluations.

Table 1
Data of MDSC of polystyrene

| $p$/s....$A$/K | $T_0$/K | $\Delta C_p^{\#}/\Delta C_p^0$ | $\gamma'$/deg | $\tau_0'$/s |
|---|---|---|---|---|
| 99....1.0 | 356 | 0.00 | 89.92 | 1.15e + 04 |
| | 357 | 0.00 | 89.75 | 3.61e + 03 |
| | 358 | 0.01 | 89.58 | 2.13e + 03 |
| | 359 | 0.01 | 89.27 | 1.23e + 03 |
| | 360 | 0.02 | 88.63 | 6.57e + 02 |
| | 361 | 0.04 | 87.59 | 3.75e + 02 |
| | 362 | 0.07 | 86.17 | 2.35e + 02 |
| | 363 | 0.10 | 84.31 | 1.58e + 02 |
| | 364 | 0.15 | 81.68 | 1.08e + 02 |
| | 365 | 0.21 | 78.12 | 7.49e + 01 |
| | 366 | 0.28 | 73.62 | 5.36e + 01 |
| | 367 | 0.38 | 67.94 | 3.89e + 01 |
| | 368 | 0.48 | 61.04 | 2.85e + 01 |
| | 369 | 0.60 | 52.85 | 2.08e + 01 |
| | 370 | 0.72 | 43.71 | 1.51e + 01 |
| | 371 | 0.83 | 34.20 | 1.07e + 01 |
| | 372 | 0.90 | 25.55 | 7.53e + 00 |
| | 373 | 0.94 | 20.47 | 5.88e + 00 |
| | 378 | 0.99 | 8.23 | 2.28e + 00 |
| | 379 | 1.00 | 3.82 | 1.05e + 00 |
| | 380 | 1.00 | 3.08 | 8.49e − 01 |
| | 381 | 1.00 | 2.08 | 5.72e − 01 |
| 60....0.6 | 356 | 0.00 | 89.93 | 7.98e + 03 |
| | 357 | 0.00 | 89.76 | 2.31e + 03 |
| | 358 | 0.01 | 89.59 | 1.34e + 03 |
| | 359 | 0.01 | 89.31 | 7.88e + 02 |
| | 360 | 0.02 | 88.82 | 4.63e + 02 |
| | 361 | 0.03 | 88.06 | 2.82e + 02 |
| | 362 | 0.05 | 86.94 | 1.79e + 02 |
| | 363 | 0.08 | 85.43 | 1.19e + 02 |
| | 364 | 0.11 | 83.46 | 8.33e + 01 |
| | 365 | 0.16 | 80.75 | 5.86e + 01 |
| | 366 | 0.22 | 77.13 | 4.18e + 01 |
| | 367 | 0.30 | 72.68 | 3.06e + 01 |
| | 368 | 0.39 | 67.06 | 2.26e + 01 |
| | 369 | 0.50 | 60.24 | 1.67e + 01 |
| | 370 | 0.61 | 52.32 | 1.24e + 01 |
| | 371 | 0.73 | 43.24 | 8.98e + 00 |
| | 372 | 0.83 | 34.07 | 6.46e + 00 |
| | 373 | 0.89 | 27.55 | 4.98e + 00 |
| | 378 | 0.98 | 10.20 | 1.72e + 00 |
| | 379 | 1.00 | 3.35 | 5.58e − 01 |
| | 380 | 1.00 | 2.50 | 4.17e − 01 |
| | 381 | 1.00 | 1.10 | 1.83e − 01 |
| 30....0.3 | 356 | 0.00 | 89.97 | 8.69e + 03 |
| | 357 | 0.00 | 89.83 | 1.56e + 03 |
| | 358 | 0.01 | 89.68 | 8.51e + 02 |
| | 359 | 0.01 | 89.41 | 4.64e + 02 |
| | 360 | 0.02 | 88.98 | 2.68e + 02 |

Table 1 (*Continued*)

| $p$/s....$A$/K | $T_0$/K | $\Delta C_p^{\#}/\Delta C_p^0$ | $\gamma'$/deg | $\tau'_0$/s |
|---|---|---|---|---|
| | 361 | 0.02 | 88.93 | 2.55e + 02 |
| | 362 | 0.04 | 87.80 | 1.24e + 02 |
| | 363 | 0.06 | 86.82 | 8.58e + 01 |
| | 364 | 0.08 | 85.71 | 6.36e + 01 |
| | 365 | 0.10 | 84.05 | 4.58e + 01 |
| | 366 | 0.14 | 81.71 | 3.28e + 01 |
| | 367 | 0.20 | 78.48 | 2.34e + 01 |
| | 368 | 0.26 | 74.83 | 1.76e + 01 |
| | 369 | 0.34 | 70.02 | 1.31e + 01 |
| | 370 | 0.44 | 63.74 | 9.68e + 00 |
| | 371 | 0.55 | 56.88 | 7.32e + 00 |
| | 372 | 0.66 | 48.73 | 5.44e + 00 |
| | 373 | 0.72 | 43.84 | 4.59e + 00 |
| | 378 | 0.97 | 13.77 | 1.17e + 00 |
| | 379 | 0.99 | 6.49 | 5.43e − 01 |
| | 380 | 1.00 | 4.43 | 3.70e − 01 |

Table 2
Data of MDSC of poly(ethylene tetrephthalate)

| $p$/s....$A$/K | $T_0$/K | $\Delta C_p^{\#}/\Delta C_p^0$ | $\gamma'$/deg | $\tau'_0$/s |
|---|---|---|---|---|
| 30....0.5 | 338 | 0.000 | 90.0 | ∞ |
| | 340 | 0.025 | 88.6 | 191 |
| | 342 | 0.052 | 87.0 | 92.2 |
| | 344 | 0.089 | 84.9 | 53.7 |
| | 346 | 0.162 | 80.7 | 29.1 |
| | 348 | 0.308 | 72.1 | 14.7 |
| | 350 | 0.549 | 56.7 | 7.27 |
| | 352 | 0.806 | 36.3 | 3.51 |
| | 354 | 0.941 | 19.7 | 1.71 |
| | 356 | 0.985 | 10.0 | 0.843 |
| | 358 | 1.000 | 0.00 | 0.00 |
| 60....1.0 | 338 | 0.000 | 90.0 | ∞ |
| | 340 | 0.027 | 88.5 | 359 |
| | 342 | 0.058 | 86.7 | 166 |
| | 344 | 0.124 | 82.9 | 76.6 |
| | 346 | 0.253 | 75.3 | 36.5 |
| | 348 | 0.481 | 61.2 | 17.4 |
| | 350 | 0.748 | 41.6 | 8.47 |
| | 352 | 0.919 | 23.2 | 4.09 |
| | 354 | 0.978 | 12.0 | 2.03 |
| | 356 | 0.995 | 5.51 | 0.921 |
| | 358 | 1.000 | 0.00 | 0.00 |

Table 2 (*Continued*)

| $p$/s....$A$/K | $T_0$/K | $\Delta C_p^{\#}/\Delta C_p^0$ | $\gamma'$/deg | $\tau'_0$/s |
|---|---|---|---|---|
| 90....1.5 | 338 | 0.000 | 90.0 | ∞ |
| | 340 | 0.027 | 88.5 | 535 |
| | 342 | 0.063 | 86.4 | 228 |
| | 344 | 0.150 | 81.4 | 94.2 |
| | 346 | 0.325 | 71.1 | 41.7 |
| | 348 | 0.582 | 54.4 | 20.0 |
| | 350 | 0.823 | 34.6 | 9.89 |
| | 352 | 0.948 | 18.6 | 4.82 |
| | 354 | 0.983 | 10.5 | 2.65 |
| | 356 | 0.995 | 5.77 | 1.453 |
| | 358 | 1.000 | 0.00 | 0.00 |

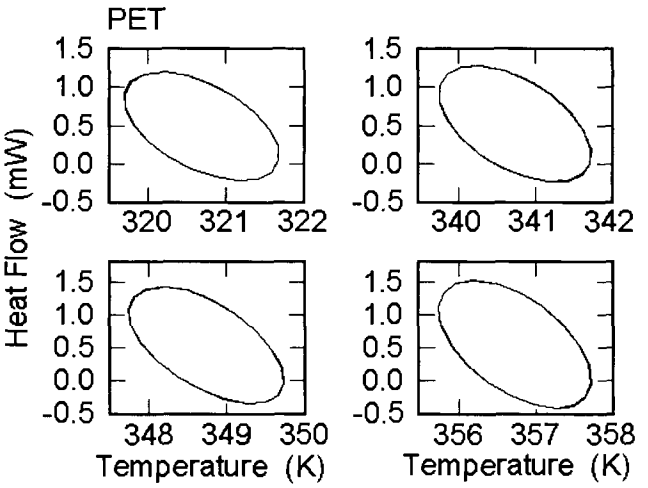


Fig. 4. Lissajous figures at four temperatures throughout the glass transition region (the modulation period is 60 s, modulation amplitude 1 K, 20 data points in each of the 10 superimposing Lissajous figures).

### 4.2. Data treatment

The measured data correspond to an apparent heat capacity and the change through the glass transition was expressed in terms of the phase-shift $\gamma$' as given by Eq. (17). Both $\Delta C_p^{\#}$ and $\Delta C_{p_0}$ were evaluated at each temperature $T_0$. The values of $\gamma$' are also shown in Tables 1 and 2. Fig. 5 illustrates the change of $\gamma$' with temperature in the glass transition region for poly(ethylene terephthalate) as an example. It changes from 90° in the glassy region to 0° in the liquid region. Figs. 6 and 7 reveal the preliminary, frequency-

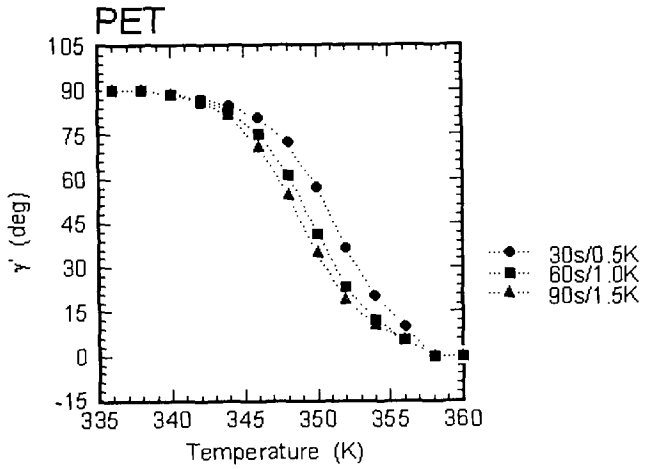


Fig. 5. Change of the phase angle $\gamma'$ with temperature for poly(ethylene terephthalate).

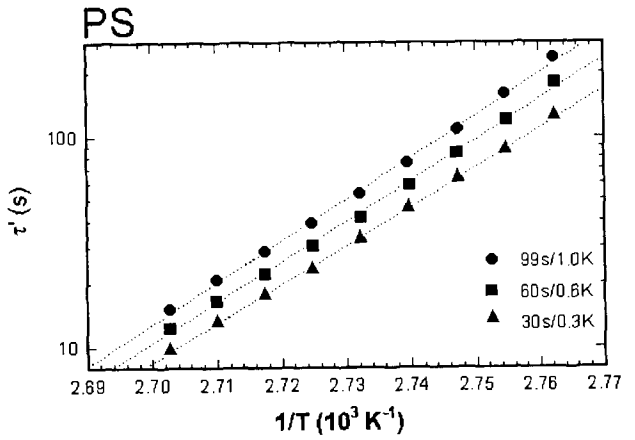


Fig. 6. Change of the logarithm of the amplitude-dependent relaxation time with inverse temperature for polystyrene.

dependent values of $\tau'$. An example of the extrapolation to zero amplitude is shown for PET in Fig. 8, and the final data for zero amplitude are shown in Figs. 9 and 10. The sets of all parameters are, finally, listed in Tables 3 and 4, and the computed apparent heat capacities as a function of frequency are drawn in Figs. 11 and 12, making use of the ATHAS data bank values for the liquid and glassy heat capacities, and covering the frequency range of 0.01–100 Hz. The computations were carried out for zero modulation amplitude using Eqs. (17) and (13).

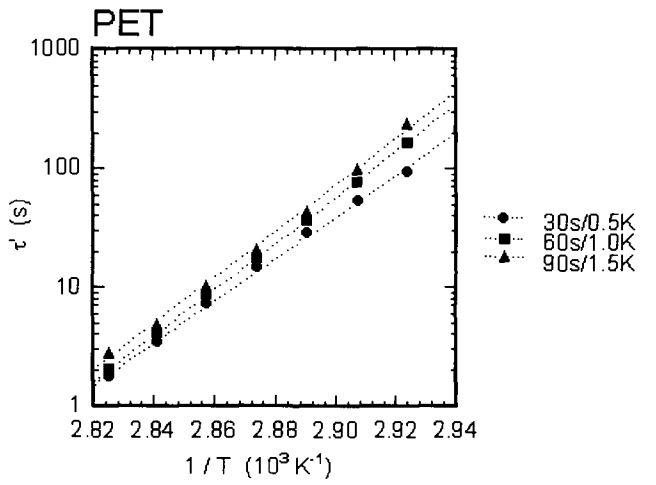


Fig. 7. Change of the logarithm of the amplitude-dependent relaxation time with inverse temperature for poly(ethylene terephthalate).

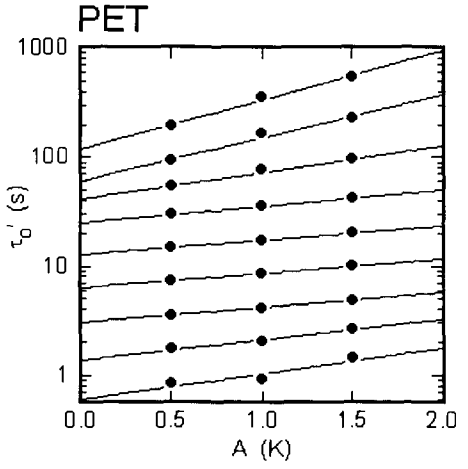


Fig. 8. Example of the extrapolation of the relaxation time $\tau_0$ to zero modulation amplitude $A$.

## 5. Discussion

Figs. (2) and (3) and the subsequent analyses show that the heat capacity from quasi-isothermal MDSC can be used to measure the frequency dependence of the glass transition. The sufficiently fast attainment of steady state can be seen from Fig. 1, and the perfect maintenance of steady state from Fig. 4. The observation that the apparent

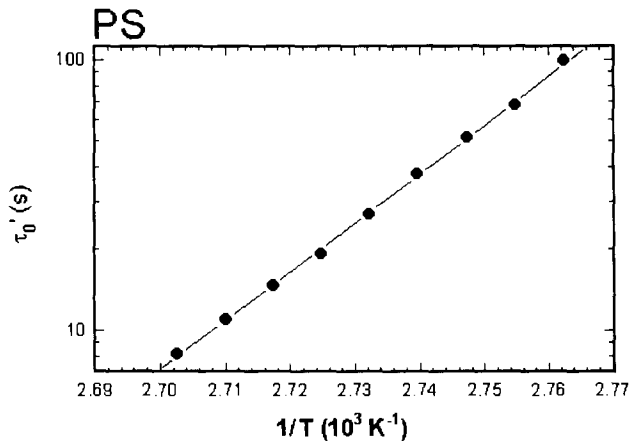


Fig. 9. Amplitude-independent relaxation time for polystyrene as a function of inverse temperature.

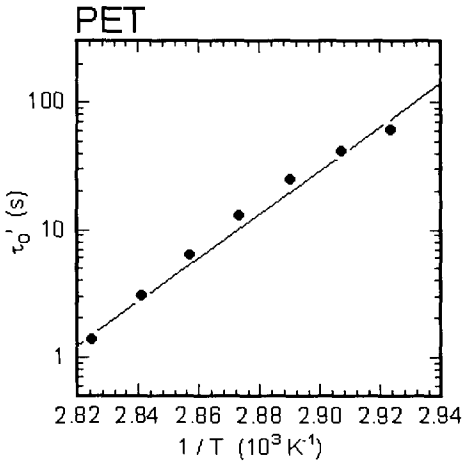


Fig. 10. Amplitude-independent relaxation time for poly(ethylene terephthalate) as a function of inverse temperature.

heat capacity is frequency dependent has already been made in a qualitative set of analyses of MDSC traces for polystyrene in the glass transition region under various modulation conditions [1]. For the first time a direct comparison with dynamic mechanical measurements can be made. The more difficult analyses with a simultaneous underlying heating rate $< q >$ that adds a second time scale will be the subject of paper IV of this series of investigations of calorimetry in the glass transition region [3].

At present, the frequency range for measurements is limited from about 0.01 to 0.1 Hz because of the need to have a negligible lag throughout the experiment and a reasonable amplitude for precision [5]. The extrapolation to 100 Hz in Figs. 11 and 12 is most

Table 3
Computed results for polystyrene in the glass transition region

| $T_0/K$ | $\tau_0/s$ | $A_N$ | $A_\tau$ | $N_0^*$/mol |
|---|---|---|---|---|
| 361 | 211 | 5.537E-3 | 0.319 | 0.927 |
| 362 | 98.3 | 5.506E-3 | 0.317 | 0.932 |
| 363 | 68.0 | 5.476E-3 | 0.315 | 0.937 |
| 364 | 51.7 | 5.446E-3 | 0.314 | 0.943 |
| 365 | 37.7 | 5.416E-3 | 0.312 | 0.948 |
| 366 | 26.9 | 5.386E-3 | 0.310 | 0.953 |
| 367 | 19.3 | 5.357E-3 | 0.308 | 0.958 |
| 368 | 14.6 | 5.328E-3 | 0.307 | 0.963 |
| 369 | 11.0 | 5.299E-3 | 0.305 | 0.969 |
| 370 | 8.2 | 5.271E-3 | 0.304 | 0.974 |
| 371 | 6.3 | 5.242E-3 | 0.302 | 0.979 |
| 372 | 4.8 | 5.214E-3 | 0.300 | 0.985 |
| 373 | 4.1 | 5.186E-3 | 0.299 | 0.990 |
| 378 | 0.92 | 5.050E-3 | 0.291 | 1.017 |
| 379 | 0.37 | 5.023E-3 | 0.291 | 1.022 |
| 380 | 0.24 | 4.997E-3 | 0.288 | 1.027 |
| 381 | 0.033 | 4.971E-3 | 0.286 | 1.033 |

In addition, $B$, the pre-exponential factor of Eq. (10) is $1.876 \times 10^{-46}$ s; the activation energy for hole formation, $\varepsilon_j$ is 345.5 kJ mol$^{-1}$; the hole energy, $\varepsilon_h$ is 6.00 kJ mol$^{-1}$; and the change of $N^*$ on modulation, $\alpha$, is $5.13 \times 10^{-3}$ mol K$^{-1}$.

Table 4
Computed results for poly(ethylene terephthalate) in the glass transition region

| $T_0/K$ | $\tau_0/s$ | $A_N$ | $\alpha/K^{-1}$ | $A_\tau$ | $N_0^*$/mol |
|---|---|---|---|---|---|
| 338 | | 4.95E-3 | 1.86E-2 | 0.346 | 3.77 |
| 340 | 119 | 4.89E-3 | 1.85E-2 | 0.341 | 3.78 |
| 342 | 61.2 | 4.83E-3 | 1.84E-2 | 0.337 | 3.80 |
| 344 | 41.5 | 4.78E-3 | 1.82E-2 | 0.334 | 3.82 |
| 346 | 24.7 | 4.72E-3 | 1.81E-2 | 0.330 | 3.83 |
| 348 | 12.7 | 4.67E-3 | 1.80E-2 | 0.326 | 3.85 |
| 350 | 6.24 | 4.62E-3 | 1.78E-2 | 0.322 | 3.86 |
| 352 | 2.99 | 4.56E-3 | 1.77E-2 | 0.319 | 3.88 |
| 354 | 1.35 | 4.51E-3 | 1.76E-2 | 0.315 | 3.89 |
| 356 | 0.605 | 4.46E-3 | 1.74E-2 | 0.311 | 3.91 |
| 358 | 0.00 | 4.41E-3 | 1.73E-2 | 0.308 | 3.92 |

In addition, $B$, the preexponential factor of Eq. (10) is $5.59 \times 10^{-49}$ s; the activation energy for hole formation $\varepsilon_j$ is 328 kJ mol$^{-1}$; the hole energy $\varepsilon_h$ is 4.70 kJ mol$^{-1}$.

certainly the limit of prediction. One expects the activation energies derived from Figs. 9 and 10 to decrease with temperature. As in dynamic mechanical measurements [1, 6], a WLF or similar temperature dependence is needed instead to Eq. (10) to extend the frequency range.

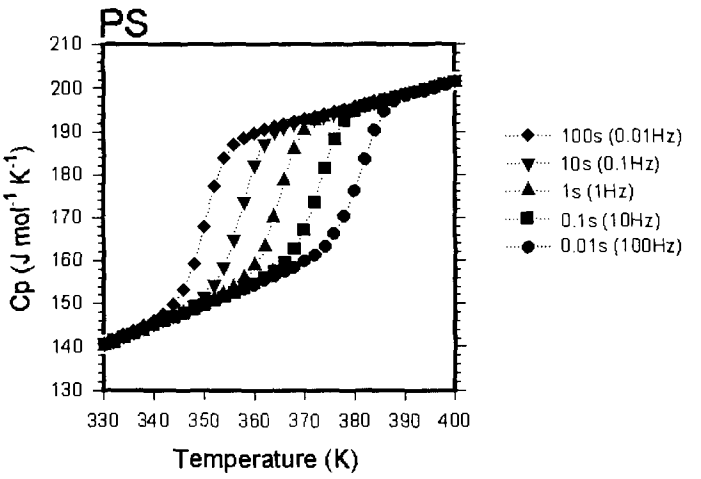


Fig. 11. Computed heat capacity of polystyrene as a function of frequency, using Eq. (15) and the parameters of Table 3 and the data bank information.

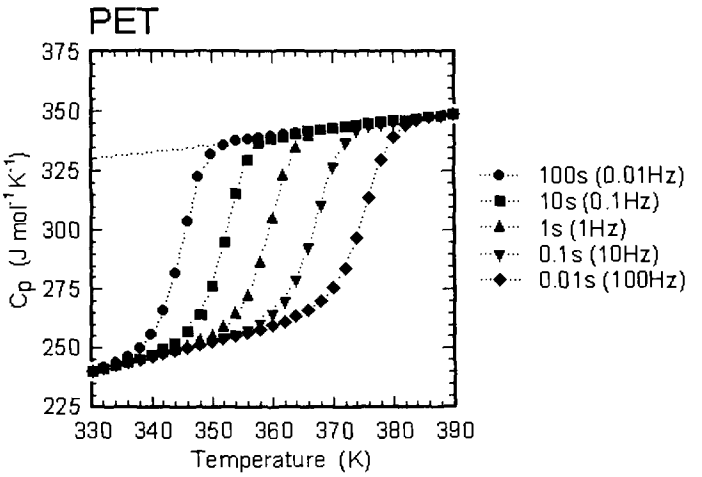


Fig. 12. Computed heat capacity of poly(ethylene terephthalate) as a function of frequency, using Eq. (15) and the parameters of Table 4 and the data bank information.

The complete heat capacity, as shown in Figs. 11 and 12, is based on two sets of experiments. One is the standard heat capacity measurements in the stable and metastable temperature ranges of the liquid and glass with maximum samples masses, as is outlined for examples in Refs. [9] and [14] (20–40 mg sample). The other is the experiment described here of the frequency-dependent measurement of the apparent

heat capacity with lower sample mass to keep a small lag (as given in Eq. (5)). For this reason, it is best to normalize the apparent heat capacities of Eqs. (16) and (17) to the more precise $\Delta C_{p_o}$ of the data bank, as done in Figs. 2 and 3.

The evaluation of the phase angle $\gamma'$ through Eq. (17) and the relaxation time from Eq. (13) as illustrated in Figs. 5–8, followed by extrapolation to zero modulation amplitude (Figs. 9 and 10) is a simple approach to obtain the hole parameters. It avoids the rather difficult complete solution of the hole equilibrium *via* Eq. (12) [7]. Eq. (16) is illustrated in Fig. 13 for $A_\tau = 0.25$ and $A_N = 1.00$ at $\gamma = 1.00$ rad (57.3°). The decreasing relaxation time at increasing temperature forces the number of holes further towards equilibrium and at decreasing temperature it retards the approach to equilibrium, as seen from the dashed lines.

The data in Tables 3 and 4 suggest the ratio $A_\tau/A_N$ to be about 100 and not 0.25 as in Fig. 13. Under such conditions, Eq. (16) does not represent the experimental data well. To check the correspondence of the hole theory concept with the MDSC, the corresponding difference equation to Eq. (8) with intervals of 1.00 s and the appropriate parameters from Tables 3 and 4 was set up and added from arbitrary $N_0$ for several modulation cycles. Fig. 14 shows the result for 350 K of PET with the modulation amplitude and period of 1.00 K and 50 s. A perfect, but asymmetric modulation can be seen between 200 and 400 s. As a next step, the MDSC average and deconvolutions were programmed beginning at 200 s. The various signals are displayed in Fig. 15. Good agreement was achieved with the calculations of Fig. 12. The heat flow $HF$(total) is $\varepsilon_h \times \Delta N$. This leads to $C_p^\# = A(HF)/(\omega A) = 8.55/0.126 = 68.0$ J K$^{-1}$ mol$^{-1}$ and compares to a zero-amplitude value in Fig. 12 of 69.7 J K$^{-1}$ mol$^{-1}$. Over the whole glass transition region, the root-mean-square agreement was ± 10%, with the larger percentage errors at low values for $C_p^\#$. The average absolute error was 1.7 K$^{-1}$mol$^{-1}$ for six data points between 340 and 358 K. All averages and smoothings in Fig. 15 are taken over the time $\pm p/2$. The detailed equations are given, for example, in Ref. [6].

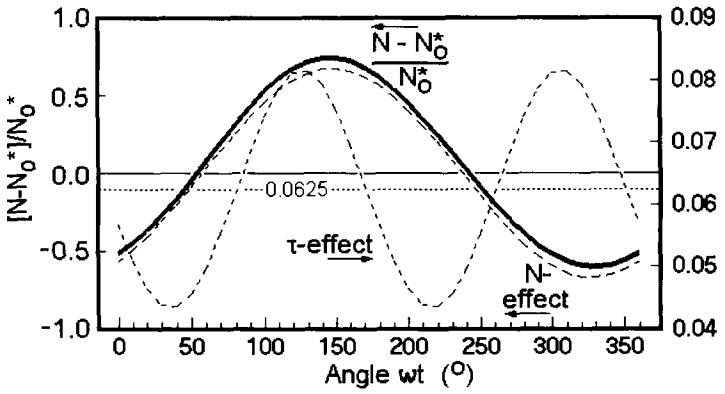


Fig. 13. Change in the number of holes during one modulation period, as given by Eq. (16). The dashed curves illustrate the effects of the two terms in the equations.

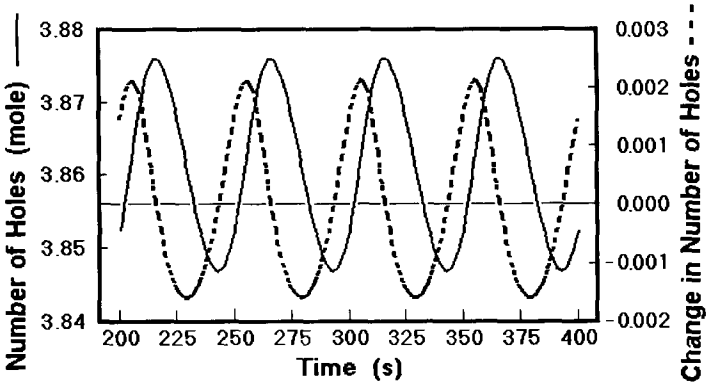


Fig. 14. Evaluation of the number of holes for PET at 350 K using the difference equation corresponding to Eq. (10) using data of Table 4. Modulation frequency, 0.02 Hz; amplitude, 1.00 K.

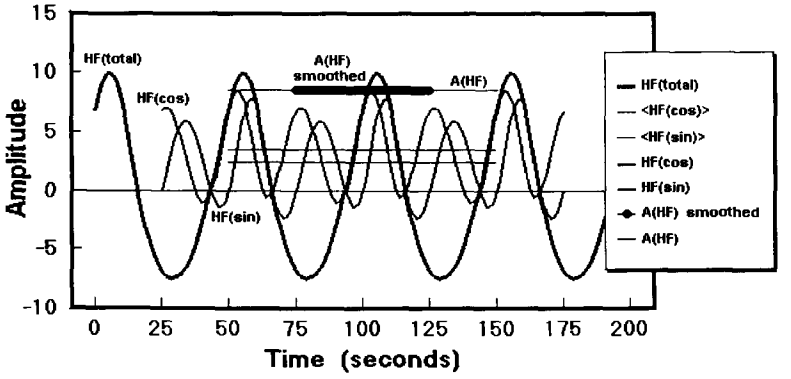


Fig. 15. Evaluation of MDSC parameters for the data of Fig. 14. The expression for the curve labeled $HF(\cos)$ is equal to $[HF(\text{total}) - <HF(\text{total})>]\cos\omega t$. An analogous expression is used for $HF(\sin)$. All average $< >$ and smoothing goes over one modulation period by sliding summation.

Fig. 15 also permits the details of the flow of the MDSC data to be followed *i.e.* once the scheme of computation has been set up in the form of a spread sheet (Lotus 1-2-3™, Release 4), any calorimetric condition can be simulated and the experimental conditions analyzed (see also Ref. [3] for more details).

## Acknowledgments

This work was financially supported by the Div. of Materials Res., NSF, Polymers Program, Grant # DMR 90-00520 and the Div. of Materials Sci., Office of Basic Energy

Sciences, U.S. Department of Energy, under DE-AC05-84OR21400 with Lockheed Martin Energy Systems. Support for instrumentation came from TA Instruments, Inc. and Mettler-Toledo, Inc. Research support was also given by ICI Paints, Exxon Res. and Eng. Co., Shell Development Co., and Toray Industries. Inc.

## References

[1] A. Boller, C. Schick and B. Wunderlich, in J.B. Enns (Ed.), Proc. 23rd NATAS Conf. Toronto, Canada, Sept. 25–28, 1994, p. 25–28; Thermochim. Acta 226 (1995) 97 part I of this series of papers.
[2] M. Reading, D. Elliot and V.L. Hill, J. Therm. Anal., 40 (1993) 949.
P.S. Gill, S.R. Sauerbrunn and M. Reading, J. Therm. Anal., 40 (1993) 931.
M. Reading, Trends Polym. Sci., 8 (1993) 248.
[3] L. Thomas and B. Wunderlich, Thermochim Acta, (1996) in print, Part IV of this series of papers.
[4] B. Wunderlich, A. Boller, I. Okazaki and S. Kreitmeier, J. Therm. Anal. (1996), in print, Part II of this series of papers.
[5] Y. Jin, A. Boller and B. Wunderlich, in K.R. Williams, (ed.), Proc. 22nd NATAS Conf., Denver, Co, September 19–22 1993, p. 59–64.
See also, A. Boller, Y. Jin and B. Wunderlich, J. Therm. Anal. 42 (1994) 307.
[6] B. Wunderlich, Y. Jin and A. Boller, Thermochim. Acta, 238 (1994) 277.
[7] B. Wunderlich, A. Boller, I. Okazaki and S. Kreitmeier, Thermochim. Acta, (1996) in print.
[8] D.A. Ditmars, S. Ishihara, S.S. Chang, G. Bernstein and E.D. West, J. Res. Natl. Bur. Stand., 87 (1982) 159.
[9] B. Wunderlich, Pure Appl. Chem., 67 (1995) 1919 Contact the authors for summaries of the data bank, or see our home page on the WWW (Internet), URL: http://funnelweb.utcc.utk.edu/~athas
[10] B. Wunderlich, D.M. Bodily and M.H. Kaplan, J. Appl. Phys., 35 (1964) 95
[11] B.G. Sumpter, D.W. Noid, G.L. Liang and B. Wunderlich, Atomistic Dynamics of Macromolecular Crystals, Adv. Polym. Sci., 116 (1994) 27–72 (Volume on Atomistic Modelling of Physical Properties of Polymers, U. Suter and L. Monnerie (Eds.)).
[12] H. Eyring, Chem. Phys., 4 (1936) 238.
J. Frenkel, Kinetic Theory of Liquids. Clarendon Press, Oxford, England, 1946.
[13] N. Hirai and H. Eyring, J. Appl. Phys., 29 (1958) 810; J. Polym. Sci., 37 (1959) 51.
[14] B. Wunderlich, Thermal Analysis, Academic Press, Boston, 1990.
[15] B. Wunderlich, The nature of the glass transition and its determination by thermal analysis, in R.G. Seyler (Ed.), Assignment of the Glass Transition, ASTM Symposium, March 4–5, 1993, Atlanta, GA. STP 1249, Am. Soc. Testing of Materials, Philadelphia, 1994, p. 75.
[16] J.D. Ferry, Viscoelastic Properties of Polymers, 3rd edn., J. Wiley, New York, NY, 1980.